J Fusion Energ (2013) 32:50–55
DOI 10.1007/s10894-012-9521-9

ORIGINAL RESEARCH

Magnetic Reynolds Number and Neon Current Sheet Structure in the Axial Phase of a Plasma Focus

S. Lee · S. H. Saw · P. Lee · R. S. Rawat · K. Devi

Published online: 6 March 2012

Abstract The Magnetic Reynolds Number (MRN) in neon is computed as a function of Neon shock speed. The magnetic field profiles at various positions in the axial run down phase of the INTI Plasma Focus device are measured over a range of pressures from 2 to 20 Torr. These profiles are assessed for good electromagnetic coupling including measuring the current per unit current sheet thickness as a comparative measure of current sheet diffusion. It was found that at an axial current sheet speed of over 3.5 cm/μs (corresponding to MRN > 15), the current sheet has a compact profile with current density of 55 kA/cm of sheet thickness whereas at speeds below 2.8 cm/μs (corresponding to MRN < 10) the profile is more diffuse with current density less than 30 kA/cm of sheet thickness. Based on these studies it is proposed to take a speed of 3 cm/μs corresponding to an MRN of 10 as the minimum speed of neon current sheet below which the electromagnetic coupling begins to weaken.

Keywords Magnetic Reynold Number · Shock speed · Plasma focus device · Current sheet diffusion

S. Lee · S. H. Saw · K. Devi
INTI International University, 71800 Nilai, Malaysia

S. Lee · S. H. Saw
Institute for Plasma Focus Studies, 32 Oakpark Drive, Chadstone 3148, Australia

P. Lee · R. S. Rawat (✉)
National Institute of Education, Nanyang Technological University, Singapore 637616, Singapore
e-mail: rajdeep.rawat@nie.edu.sg

Introduction

The use of neon in a plasma focus is important because of the intense radiation achievable, particularly in soft X-ray (SXR) regime, which has several applications [1–6]. The predominant spectrum that is radiated from a neon operated plasma focus device depends on the radial phase speed which has a particular relationship to the axial phase speed dependent on the radius ratio and specific heat ratio. For example, for soft X-ray lithography [1–3] the characteristic neon SXR line radiation around 1–1.3 nm is required. Modelling [7, 8] of plasma dynamics in plasma focus device shows that this requires a radial collapse speed of around 25 cm/μs which is driven from the final axial speed of around 7 cm/μs at the end of the axial phase, in a geometry such as that of the UNU/ICTP plasma focus facility (PFF). In its early axial phase the current sheet speed is much lower. In some special geometries, such as tapered or reducing composite anodes [9], the current sheet speed is kept particularly low for a fair portion of its early axial phase. These speeds could be as low as 2 cm/μs. There is evidence that in argon [5] operation when the axial current sheet speed is around 3 cm/μs the Magnetic Reynolds Number (MRN) may be already too low for a good electromagnetic drive [10] characterized by a diffusive current sheet. In this paper, we investigate the effectiveness of a neon current sheet as an efficient driver at axial current sheet speeds as low as 2 cm/μs.

Theory

The condition for efficient electromagnetic drive in which energy is deposited into a plasma flow by a magnetic field—flow field convective mechanism rather than by

Joule heating, may be shown by dimensional analysis of the induction equation to be:

$$\mu\sigma v l \gg 1 \tag{1}$$

where μ is the permeability of the plasma (generally the same as the permeability of free space); σ is the electrical conductivity; v the flow speed and l the characteristic length of the change in the driving magnetic field. The quantity $R_m = \mu\sigma v l$ is known as the Magnetic Reynolds Number (MRN). For electromagnetic shock tube operation, a major parameter is the shock speed q_1. It is useful to note the dependence of R_m on q_1. This may be obtained as follows. Following Spitzer [11], we may write an expression for the plasma electrical conductivity:

$$\sigma = \frac{1}{65.3\ln(\Lambda)Z} T_e^{3/2} \tag{2}$$

where Λ = (Debye length λ_D)/(90° impact parameter b_0) and Z (also refereed as effective charge number Z_{eff}) is the charge number of the plasma having electron temperature T_e, assuming the plasma to be in thermal equilibrium.

Noting that at 2 cm/μs the Mach number in neon is in excess of 40 and so one can apply the strong shock wave jump equations [12] and obtain plasma temperature of:

$$T_c = 2.4 \times 10^{-4} M \frac{(\gamma-1)}{(\gamma+1)^2} \frac{q_1^2}{D} \tag{3}$$

where γ is the specific heat ratio, M the molecular weight of the plasma gas species and the departure coefficient $D = 1 + Z$.

Thus we may write, the MRN as:

$$R_m = C \frac{(\gamma-1)^{3/2}}{(\gamma+1)^3} \frac{l}{\ln(\Lambda) Z (Z+1)^{3/2}} q_1^4 \tag{4}$$

where $C = 0.72 \times 10^{-13}\ M^{3/2}$ if we take q_1 as the plasma flow speed. This is a reasonable approximation.

Equation (4) indicates a rapid increase of R_m with q_1 ($R_m \cong q_1^4$) for a given l if the thermodynamic function γ and Z are constant, as is for perfect gas. For real gases, however, γ and Z, along with the shock speed q_1, also have a big influence on the MRN function, R_m.

The thermodynamic function γ may be taken to be an indicator [13] of the degree of freedom f. We may write $\gamma = (2 + f)/f$ so that $\gamma \to 1$ in the case where $f \to \infty$. This is a gas with a large heat capacity, difficult to heat up as can be seen from (3) where as $\gamma \to 1$, $T \to 0$. As an example, for a gas such as neon in its freely ionizing regime [13] (i.e. not approaching any ionization limits) we compute using a corona model that $\gamma \sim 1.2$ with $f \sim 10$. This compares with the perfect gas case with $\gamma = 5/3$ and $f = 3$. Thus as neon gets heated sufficiently to begin ionizing, the reduction of the value of γ below 5/3, towards 1, tends to decrease the rapid increase of R_m with the shock speed q_1 as evident from (3).

Further, as the neon plasma gets heated to higher temperatures the values of Z will increase due to increasing ionization and continue to increase, with increasing temperatures to a limit of Z = 10 at greater than 10 million K. This increase of Z with temperature tends to further reduce the rapidity of the increase in R_m with the shock speed.

To demonstrate the dependence of R_m on the shock speed q_1 and the real gas effects on this dependence, Z and γ are computed [13] as a function of T for neon using, as an approximation, the corona model [14]. The value of R_m^* (the value of R_m referenced to $l = 1$ cm) is then computed over a range of temperatures (or over a range of q_1 by the use of (3)) to adequately contrast regimes where the gases are real with regimes where the gases are near perfect. The resulting curve of R_m^* is shown in Fig. 1. Also shown is the charge number Z (or Z_{eff}) scaled up 10 times for a better display. From Fig. 1, it is noted that neon ionization rises significantly above zero at shock speed of 1 cm/μs (around a shock Mach number of 30) and continues to rise strongly until Z reaches a closed shell value of 8 at 14 cm/μs (plasma shock temperature T of 5.7×10^5 K), stays at 8 as the shock speed increases to 22 cm/μs ($T = 2 \times 10^6$ K) and then starts rising again relatively slowly reaching only 8.2 at 26 cm/μs (2.8×10^6 K). Only when the speed reaches 50 cm/μs (9×10^6 K) does neon reach practically full ionization with Z approaching 10. The value of R_m^* is 3.1 at 2 cm/μs, rises relatively slowly to 5 at 3 cm/μs, rises more rapidly to 10 at 4.5 cm/μs, reaches 57 at 10 cm/μs and continues rising rapidly at higher shock speeds. Magnetic probe measurements in electromagnetic shock tubes [15] typically show current sheet widths of 2–4 cm, so we may estimate that in the range of 2–3 cm/μs the effective value of R_m is typically around 6–15. This would be an interesting region to investigate as it would be the

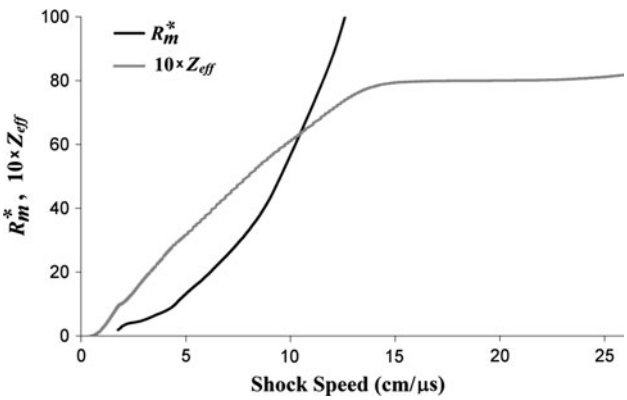

Fig. 1 Computed R_m^* and Z_{eff} (or Z) as a function of shock speed in neon

transition region at which the diffusive (Joule heating) mechanisms would start becoming apparent.

Experimental Set Up

The INTI PF [16] is one of the machines in the network of UNU ICTP PFF [7, 16]. It is powered by a 30 μF, 15 kV fast discharge capacitor which is discharged through a parallel-plate swinging-cascade spark-gap onto a plasma focus tube housing the coaxial electrode assembly comprising of 16 cm long anode/cathode of radii 0.95/3.2 cm. The anode is a solid piece with a slightly rounded end whose centre is engraved with a 1 cm deep pit of 1 cm diameter. The cathode is formed of a ring of six 1-cm diameter rods.

Three magnetic probes of 10 turns each wound on a 1 mm diameter former are positioned, inside a 3 mm diameter thin-wall glass tube, at positions of 0.2, 4.2 and 8.4 cm from the sealed end of a glass tube. The tube is inserted via a vacuum-sealed aperture into the annular region, midway in the 2.2 cm channel between the anode and the 'squirrel-cage' cathode. The 3 magnetic field sensing coils are all oriented in the same direction (with the axis of a coil tangential to the circular cross-section) in order to detect the azimuthal magnetic field of the current flowing through the anode feeding and driving the current sheet down the axial phase of the plasma focus. The axial positions of the coils are fixed for a series of shots at different pressures. Then the positions are moved and fixed for another series of shots at different pressures.

For each shot the rate of change of magnetic field (dB/dt) of the 3 probes are recorded on 3 channels of a 4-channel 350 MHz Digital Storage Oscilloscope (DSO) at 1 GSa/s with a record length of 10,000 points. The signal from a 3-turn coil (measuring the rate of change of current, dI/dt) wrapped around the earth return of one of the 16 coaxial cables carrying the discharge current, is displayed on the fourth channel of the DSO. The digital data of the 4 channels are then integrated numerically and any integrated baseline shift of each channel is fitted with a linear equation and subtracted from the integrated signal.

Results and Discussion

Axial Trajectory Speed Measurements

The 4 integrated, baseline corrected, signals of a typical plasma focus shot are shown in Fig. 2. Figure 2 shows oscilloscope traces for plasma focus shot at 2 Torr with the current in the top trace rising to a peak value of 155 kA at 2.95 μs. No focus current dip is apparent in this shot although at 2 Torr typically a strong current dip would appear. This is due to the presence of the magnetic probe creating an asymmetry in the driving current sheet inhibiting the formation of the focus. The first probe placed at position 3.2 cm from the starting end of the axial phase (i.e. the back-wall plate at closed end of coaxial electrode assembly) detects the arrival of the current sheet at 1.61 μs from the start of the current. The time of arrival of the current sheet is taken as the point where the magnetic field turns from a slow rise to a much sharper rise. The second probe at 7.2 cm records the arrival of the current sheet at 2.68 μs; whilst the third probe at 11.4 cm records arrival time instant as 3.67 μs.

The Lee model code [7–9, 14, 16] was used to compute the axial phase trajectory. It was found that a bigger than normal axial mass factor of 0.09 was required for the current fit and even then the computed trajectory still

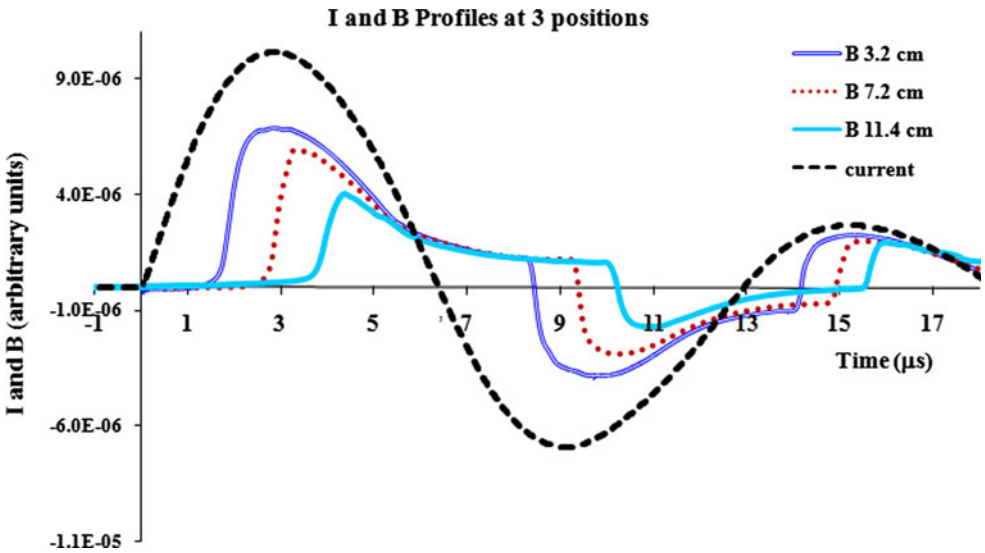

Fig. 2 Oscilloscope traces for shot S2@ 2 Torr neon. Four traces from *left* to *right*: current and magnetic coils at positions 3.2, 7.2 and 11.4 cm

showed a faster current sheet than the experimental curve obtained from the 4 experimental points (including the zero point) and then fitted with a third-order polynomial. This was another indication of probe interference with the flow. The results are shown in Fig. 3.

Similar analysis with other sets of data reveals that for the higher pressures the flow interference of the probe appears to be far less significant. For example, a set of data for 15 Torr neon is shown in Fig. 4.

The resultant comparative graph for axial phase trajectory is shown in Fig. 5. The agreement between the computed and the experimentally measured trajectories is very good, much better than the one fitted for the case of 2 Torr neon. Moreover the axial model parameters, the axial mass and current factors, used for this case are the normal values of 0.05 and 0.7, respectively.

The comparison of measured and computed trajectories thus shows that at higher neon operating pressures the flow is not significantly affected by the insertion of the magnetic probe. We show in Fig. 6 another set of current and magnetic probe signals obtained for an intermediate pressure of 10 Torr of neon.

Current Density as an Indicator of Effectiveness of Magnetic Field Coupling to the Current Sheet

From analysis of 50 sets of data it was decided that the effectiveness of the electromagnetic drive should be studied not too close to the starting end of the axial phase since there is then the lift-off mechanism and the sheet formation region to be considered and these effects will interfere with the study of the effect of the Magnetic Reynolds Number (MRN). Thus it was decided to avoid the region less than 6 cm from the starting end of the axial phase. The study

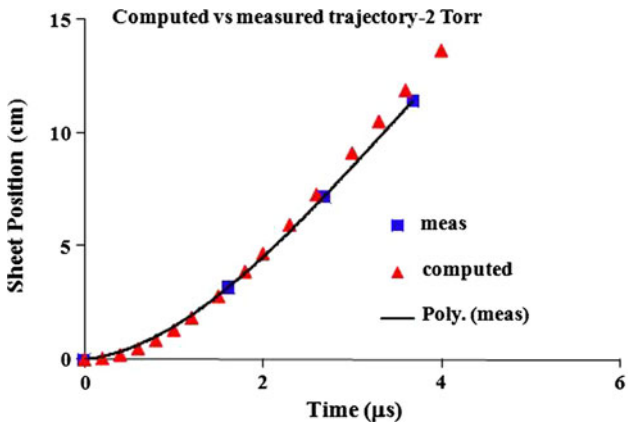

Fig. 3 Experimental axial phase trajectory compared to computed trajectory for 2 Torr neon operation

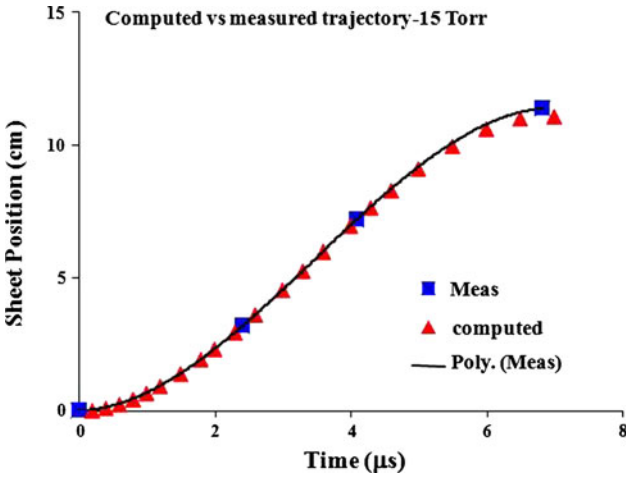

Fig. 5 Experimental axial phase trajectory compared to computed trajectory for 15 Torr neon operation

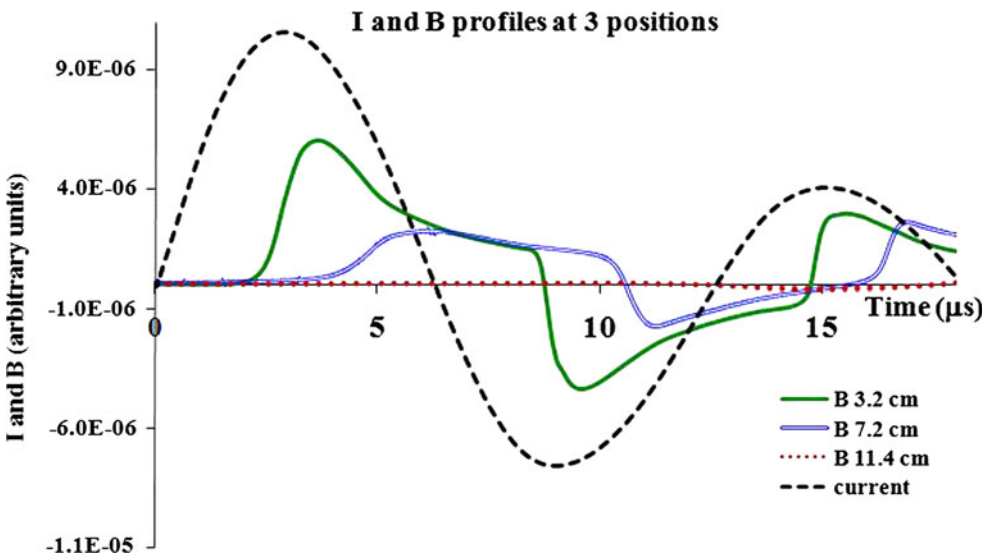

Fig. 4 Oscilloscope traces for shot S23@ 15 Torr neon. Four traces from *left* to *right*: current and magnetic coils at positions 3.2, 7.2 and 11.4 cm

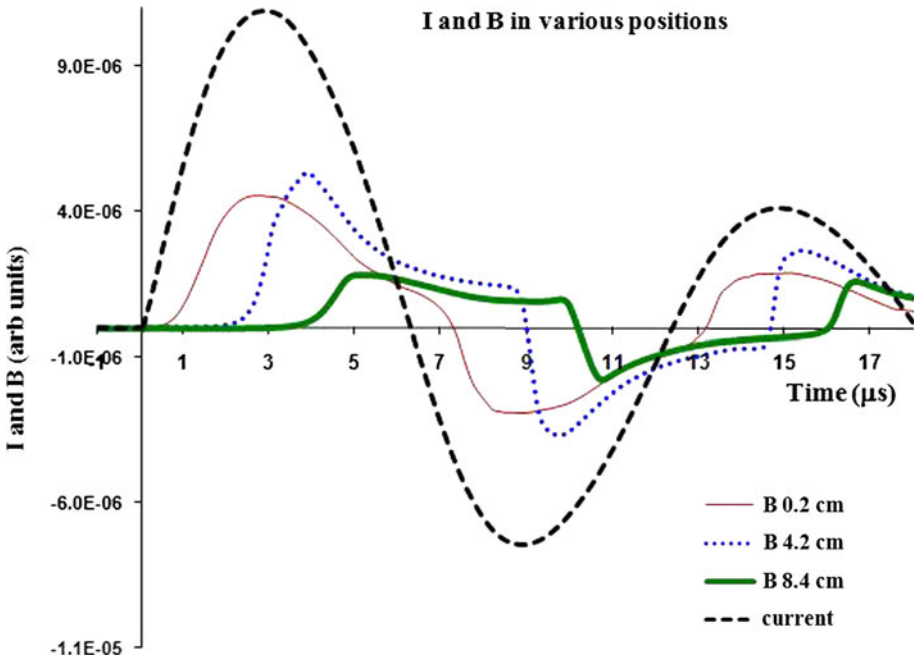

Fig. 6 Oscilloscope traces for shot S3@ 10 Torr neon. Four traces from *left* to *right*: current and magnetic coils at positions 0.2, 4.2 and 8.4 cm

would also exclude the region where the current has dropped too close to the zero value; since in that region (between the time when the tube voltage has dropped to zero and the start of the reverse current sheet) it is known that a closed current loop is formed [15]. This closed current loop is also apparent in our probe signals noting that the probes continue to show positive magnetic field after the capacitor current has reversed (see Figs. 2, 4, 6). These 3 figures show the presence of a remnant current circulating in a closed loop in front of the reversed current sheet. This closed loop of current carrying the remnant (estimated to be about 10% of the peak positive current) is decoupled from the capacitor bank and is pushed ahead of the new current sheet driven by the second half cycle of negative current. To avoid the complications of the closed current loop, it was decided not to consider the current sheets arriving after 4.1 μs.

Table 1 Experimentally estimated arrival time, speed, and thickness of the current sheet at different probe positions at different neon pressures

Shot no.	Pressure (Torr Ne)	Arrival time instant (μs)	Sheet position (cm)	*dz/dt* (cm/μs)	Current/cm of sheet thickness (kA/cm)
S23a	15	4.09	7.20	2.32	20.3
S22a	15	3.94	7.20	2.40	35.0
S5a	10	3.58	7.20	2.80	30.3
S3c	10	3.95	8.40	2.58	34.0
S10c	3	2.69	8.40	3.64	54.7
S2a	2	2.69	7.20	4.09	57.2

From the set of results, we selected those that fit into the above criteria and display the results in Table 1. The Table 1 shows the current sheet arrival times at the probe position, the speed of the current sheet at that position and the current per cm of sheet thickness. The sheet thickness was estimated from the risetime of the magnetic field multiplied by the speed of the current sheet.

In the Table 1, the shots at 2 and 3 Torr are taken as the reference for good electromagnetic coupling since the speed at the observing positions are above 3.5 cm/μs so that the typical MRN should be above 20 (Fig. 1). The current per cm of current sheet thickness for these two shots are estimated as about 55 kA/cm. We then note that for the higher pressure shots at 10–15 Torr the speeds at similar axial positions are lower, ranging from 2.3 to 2.8 cm/μs. At these lower speeds it is noted that the current per cm of current sheet thickness ranges from 20 to 35 kA/cm. It is also noted that at this range of speeds; the calculations shown in Fig. 1 and discussed above indicate a MRN of less than 10.

Comparing the profiles of e.g. second probe of Fig. 4 (20 Torr) and third probe of Fig. 6 (10 Torr) with current sheets at lower speeds and comparing these profiles with those of the faster current sheet of the first and second probes for Fig. 1, it may be noted that the profiles of the slower current sheet are appearing less sharp which could be an indication that they are beginning to be diffusive. This is confirmed through the measurements of the current densities. We have established that in our operational range, strong electromagnetic coupling is observed at current sheet speeds above 3.5 cm/μs corresponding to MRN above 20 with current density of the order of 55 kA/cm of current sheet

thickness. At speeds below 2.8 cm/μs the current density has dropped to a value below 35 kA/cm with a corresponding MRN below 10. The strong dependence of the MRN on plasma flow speed and the thermodynamic state of the gas as indicated by (4) and Fig. 1 is consistent with the results of our experiments.

Conclusions

For electromagnetically driven current sheets in Neon strong electromagnetic coupling may be expected at speeds over 3.5 cm/μs whilst below 2.8 cm/μs the coupling has already become less efficient and the current sheet shows definite signs of increased diffusiveness. The transition point may be conveniently taken as 3 cm/μs with an estimated Magnetic Reynolds Number of about 10 at that speed. This result may be useful as a guide in the low-speed operation in Neon of electromagnetic devices such as shock tubes, plasma focus and the pinch.

References

1. S. Lee, P. Lee, G. Zhang, X. Feng, V.A. Gribkov, L. Mahe, A. Serban, T.K.S. Wong, IEEE Trans. Plasma Sci. **26**, 1119 (1998)
2. D. Wong, A. Patran, T.L. Tan, R.S. Rawat, P. Lee, IEEE Trans. Plasma Sci. **32**, 2227 (2004)
3. Y. Kato, I. Ochiai, Y. Watanabe, S. Murayama, J. Vac. Sci. Technol. B **6**, 195 (1988)
4. F.N. Beg, I. Ross, A. Lorena, J.F. Worley, A.E. Dangor, M.G. Hanies, J. Appl. Phys. **88**, 3225 (2000)
5. R.S. Rawat, T. Zhang, G.J. Lim, W.H. Tan, S.J. Ng, A. Patran, S.M. Hassan, S.V. Springham, T.L. Tan, M. Zakaullah, S. Lee, P. Lee, J. Fusion Energ. **23**, 49 (2004)
6. V.A. Gribkov, A. Srivastava, P.L.C. Keat, V. Kudryashov, S. Lee, IEEE Trans. Plasma Sci. **30**, 1331 (2002)
7. S.H. Saw, P.C.K. Lee, R.S. Rawat, S. Lee, IEEE Transc. Plasma Sci. **37**, 1276 (2009)
8. S. Lee, R.S. Rawat, P. Lee, S.H. Saw, J. Appl. Phys. **106**, 023309 (2009)
9. D. Wong, P. Lee, T. Zhang, A. Patran, T.L. Tan, R.S. Rawat, S. Lee, Plasma Sour. Sci. Tech. **16**, 116 (2007)
10. S. Lee, S.H. Saw, Abdelmagid, A. Elfetouri, A.M. Shengher, E.O. Shummaki, N.A. Hassan, J. Fiz. Malaysia **12**, 25–29 (1991)
11. L. Spitzer, *Physics of Fully Ionized Gases*, 2nd edn. (Interscience, New York, 1962)
12. R.A. Gross, in *The Physics of Strong Shock Waves in Gases in Physics of High Energy Density* ed. by P. Caldirola, H. Knoepfel (Academic Press, New York, 1971)
13. S. Lee, Aust. J. Phys. **36**, 891–895 (1983)
14. S. Lee, *Radiative Dense Plasma Focus Computation Package: RADPF*. (2011) http://www.plasmafocus.net
15. S. Lee, M. Eissa, A.V. Gholap, K.H. Kwek, S. Mulyodrono, S. Sapru, A.J. Smith, T.Y. Suryadi, W. Tou, C.S.Wong Usada, Mohammad Zakaullah, Singapore J. Phys. **3**, 75–82 (1986)
16. S.H. Saw, S. Lee, F. Roy, P.L. Chong, V. Vengadeswaran, A.S.M. Sidik, Y.W. Leong, A. Singh, Rev. Sci. Instrum. **81**, 053505 (2010)